JCTC Journal of Chemical Theory and Computation

Article

pubs.acs.org/JCTC

Describing Excited State Relaxation and Localization in TiO_2 Nanoparticles Using TD-DFT

Enrico Berardo,[†] Han-Shi Hu,[‡] Hubertus J. J. van Dam,[‡] Stephen A. Shevlin,[†] Scott M. Woodley,[†] Karol Kowalski,[‡] and Martijn A. Zwijnenburg*[,†]

[†]Department of Chemistry, University College London, 20 Gordon Street, WC1H 0AJ London, U.K.

[‡]William R. Wiley Environmental Molecular Science Laboratory, Battelle, Pacific Northwest National Laboratory, K8-91, P.O. Box 999, Richland, Washington 99352, United States

Supporting Information

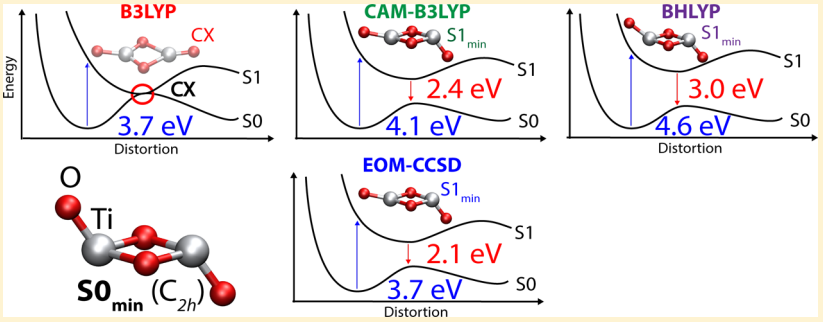

ABSTRACT: We have investigated the description of excited state relaxation in naked and hydrated TiO_2 nanoparticles using Time-Dependent Density Functional Theory (TD-DFT) with three common hybrid exchange-correlation (XC) potentials: B3LYP, CAM-B3LYP and BHLYP. Use of TD-CAM-B3LYP and TD-BHLYP yields qualitatively similar results for all structures, which are also consistent with predictions of coupled-cluster theory for small particles. TD-B3LYP, in contrast, is found to make rather different predictions; including apparent conical intersections for certain particles that are not observed with TD-CAM-B3LYP nor with TD-BHLYP. In line with our previous observations for vertical excitations, the issue with TD-B3LYP appears to be the inherent tendency of TD-B3LYP, and other XC potentials with no or a low percentage of Hartree−Fock like exchange, to spuriously stabilize the energy of charge-transfer (CT) states. Even in the case of hydrated particles, for which vertical excitations are generally well described with all XC potentials, the use of TD-B3LYP appears to result in CT problems during excited state relaxation for certain particles. We hypothesize that the spurious stabilization of CT states by TD-B3LYP even may drive the excited state optimizations to different excited state geometries from those obtained using TD-CAM-B3LYP or TD-BHLYP. Finally, focusing on the TD-CAM-B3LYP and TD-BHLYP results, excited state relaxation in small naked and hydrated TiO_2 nanoparticles is predicted to be associated with a large Stokes' shift.

INTRODUCTION

Titania (TiO_2) is the archetypal watersplitting photocatalyst[1−6] and semiconductor material for dye-sensitized solar cells.[7,8] In its use as a photocatalyst, absorption of light excites electrons from the valence band of the material to the conduction band, which leaves holes in the former and results in the creation of excited electron−hole pairs (excitons). These excitons can then, either directly or after having been ionized into "free" electrons and holes, reduce protons to hydrogen and oxidize water to oxygen. The excitons can, however, also annihilate, i.e. excited electrons and holes recombine, or become trapped. Similar processes take place in dye-sensitized solar cells, where electrons are excited from the highest occupied molecular orbital to the lowest unoccupied molecular orbital of the dye and subsequently transferred to the semiconductor (i.e., titania), while the formed holes react with a redox mediator in solution.

Overall, the physics and chemistry involved in those processes are often complicated, with the quantum efficiency−the fraction of photons absorbed resulting in the desired process taking place−depending strongly on the material properties. Recent studies, for example, show that photocatalytic activity does not only depend on the material's composition (e.g., doping level) but that both particle size and shape can play a pivotal role in controlling the fate of excitons in TiO_2.[9−16] Hence, it is crucial to properly understand the behavior of both excitons and free charge carriers (free electrons, holes) in titania. This is hard to achieve by experiment alone, for instance, because of the transient nature of excitons and/or the complex structures of samples. Computational chemistry can thus make a potentially

Received: August 28, 2014

   dx.doi.org/10.1021/ct500787x | J. Chem. Theory Comput. XXXX, XXX, XXX−XXX

significant contribution to our understanding of these systems. For the potential of computational chemistry to be realized, however, one should be able to make relatively accurate predictions of not only the optical absorption spectra, which is routinely done,[17−28] but also the reduction potentials of the free charge carriers and excitons[29−33] as well as the energetics and the structural distortion associated with trapped excitons.[34−43] Such properties require the calculation of not only vertical excited state energies but also the energies and geometries of relaxed excited states. The method of choice for calculating such properties is a combination of Density Functional Theory (DFT), for ground state energies and structures, and Time-Dependent DFT (TD-DFT), for their excited state counterparts. Alternative approaches exist in the form of quantum chemical wave function or Green's function based methods. Such alternatives have advantages in terms of reliability and inherent accuracy but unfortunately lack currently the desired scaling with system size and/or the ease of use of (TD-)DFT. This is especially true when studying the nanostructured materials relevant to applications in photocatalysis and dye-sensitized solar cells, where one has to be able to calculate the properties of systems composed of tens to hundreds of atoms.

DFT and TD-DFT are both formally exact theories; in the sense that their use formally yields the exact solution to the (excited state) many-body Schrödinger equation, but in practice one has to use an approximation for the unknown exchange-correlation (XC) potential. Results obtained will be dependent on the approximation chosen. Previously, we studied the suitability of TD-DFT for predicting vertical excited states of naked titania nanoparticles by a comparison of TD-DFT and coupled-cluster (CC) theory results.[28] We considered a range of particles that were small enough to be treated by both TD-DFT and CC methods: $(TiO_2)_n$ tentative global minimum (GM) nanoparticles, with n = 1−10 (see Figure 1),[19,44−49] and a variety of XC potentials, including a straight GGA XC potential (PBE),[50] hybrid XC potentials (B3LYP, BHLYP)[51] and a range-separated hybrid XC potential (CAM-B3LYP).[52] We found that the predicted absorption onsets, the lowest vertical excitation energies, rigidly shift up in energy with the percentage of Hartree−Fock like exchange (HFLE) included in the XC potential (PBE 0%, B3LYP, 20%, BHLYP, 50%, and CAM-B3LYP with 19% at short-range and 65% at long-range) and that TD-B3LYP and TD-CAM-B3LYP give the best quantitative fit to CC results. However, for certain nanoparticles, $(TiO_2)_3$ and $(TiO_2)_{10}$, TD-PBE and TD-B3LYP were observed to severely underestimate the absorption onset. In specific cases, TD-DFT calculations using PBE and B3LYP also predicted a different chemical character of the low-energy excited states than TD-DFT calculations using XC potentials with a higher percentage of HFLE as well as distinctly different low-energy features in the particle's absorption spectra. We demonstrated that the issue at play here is the well-known charge transfer (CT) problem of TD-DFT, where XC potentials with no or low percentages of HFLE dramatically underestimate the excitation energies of CT excitations.[28,53]

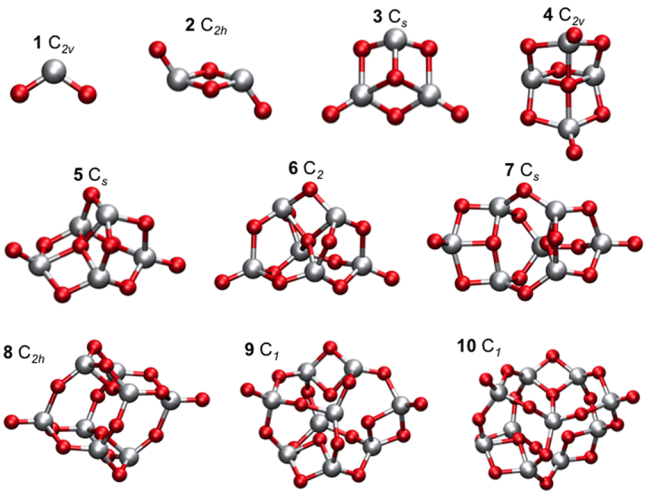

Figure 1. S0 tentative global minimum energy geometries of the TiO_2 to $(TiO_2)_{10}$ particles. Red spheres denote oxygen atoms, whereas gray represent titanium atoms. The point group symmetry of each particle is given in the label above the structure.

In this article we extend our previous work by exploring the effect of the choice of XC potential on the nature of the lowest singlet excited state (S1) minima found. We explore the S1 potential energy surface in the downhill direction, as determined from the TD-DFT analytical gradients, in order to find the S1 minima in the so-called Franck−Condon region and, subsequently, characterize these minima in terms of their photoluminescence (PL) energy and Stokes' shift (see Figure 2A). In some cases we will also find what appears to be conical intersections (CXs), where the ground and excited state potential energy surfaces touch and the PL energy goes to zero (see Figure 2B). We limit ourselves to calculations using TD-B3LYP, TD-BHLYP, and TD-CAM-B3LYP; omitting TD-PBE, as the TD-PBE vertical excitations are by far the furthest away from the CC benchmarks. For the smaller $(TiO_2)_2$ particle, we are also able to compare the predictions of TD-DFT with that of equation-of-motion CC theory with singles and doubles (EOM-CCSD).[54,55] Using this approach, we will show here that TD-CAM-B3LYP and TD-BHLYP make very similar predictions regarding the geometries and properties of the S1 minima of titania nanoparticles, which, moreover, in the case of $(TiO_2)_2$ agrees with results obtained using EOM-CCSD, whereas employing TD-B3LYP yields drastically different results. While the particles used in this study are by necessity smaller than those studied experimentally we believe that the methodological issues discussed here are independent of size-range.

COMPUTATIONAL DETAILS

Following on from our previous work, the excited state properties of TiO_2 nanoparticles were studied using a combination of ground state DFT and excited state TD-DFT. DFT is used for the energy minimization of the ground state singlet (S0) geometries and for the calculation of the harmonic frequencies of the obtained geometries, to verify that the obtained stationary points indeed correspond to minima on the S0 potential energy surface (PES). TD-DFT is then used for the calculation of the vertical excitation energies for each S0 minimum. Finally, the geometry of the lowest singlet excited state (S1) of each particle is relaxed using TD-DFT to obtain the S1 minimum energy geometry, and harmonic frequency calculations are performed on these geometries to verify that the stationary points obtained are indeed minima on the S1 surface. In our study we focus on the lowest singlet excitation, as this state, following Kasha's principle,[56] is the likely source of fluorescence (luminescence) emitted by the nanoparticle as well as the state relevant to photocatalysis.

dx.doi.org/10.1021/ct500787x | J. Chem. Theory Comput. XXXX, XXX, XXX−XXX

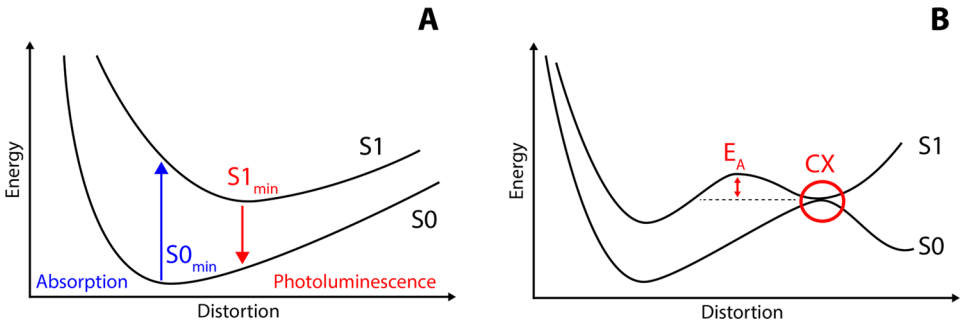

Figure 2. Cartoon of the ground (S0) and lowest excited state (S1) energy surfaces and special points thereon for the case of absorption followed by photoluminescence (A) and a conical intersection (CX) where the two surfaces touch (B). Please note that in the case of the CXs found with TD-B3LYP there is no barrier separating the CX from the ground state geometry ($E_A = 0$).

All the DFT/TD-DFT calculations are performed using the GAMESS US code (version first May 2013) and employ the def2-TZVP[57] basis set and a range of different XC potentials: the hybrid B3LYP and BHLYP XC potentials and the range-separated CAM-B3LYP XC potential. The same XC potential was used for geometry optimization and the calculation of vertical excitations. For all the ground and excited state energy minimizations the convergence criteria for the maximum Cartesian component of the gradient is chosen to be equal to 1×10^{-4} Hartree Bohr^{-1}. For a subset of nanoparticles, the TD-DFT calculations were repeated using the Turbomole 6.5 code[58−61] in order to obtain the TD-B3LYP and TD-BHLYP excited state−ground state density difference plots. Such calculations gave the same geometries and (excitation) energies as obtained using GAMESS US.

For the specific case of the $(TiO_2)_2$ GM nanoparticle, we also relaxed both the S0 and S1 geometries with the EOM-CCSD. The EOM-CCSD calculations employed, for reasons of numerical tractability, the def2-SV(P) split-valence basis set.[62] All EOM-CCSD were performed using the Tensor Contraction Engine (TCE) module of the NWChem 6.3 code.[63]

The naked structures considered are the tentative GM structures of $(TiO_2)_n$ particles for $n = 1-10$ and are shown in Figure 1. We also consider a small number of hydrated particles, see Figure 3, which were obtained through the saturation of all the undercoordinated titanium and oxygen atoms present in the naked particles with hydroxyl groups and protons, respectively. Here, we assumed that titanium atoms are normally coordinated by at least four oxygen atoms that form at least two bonds. These structures were already discussed in our previous paper, where the interested reader can find the B3LYP/def2-TZVP S0 optimized geometries. Cartesian coordinates for the S1 excited state minimum geometries obtained in this study, calculated with the different XC potentials, are listed in the Supporting Information (section ESI-1 and ESI-2). For the graphic representations of the $(TiO_2)_n$ nanoparticles and excited state−ground state density differences we used the VMD visualization software.[64]

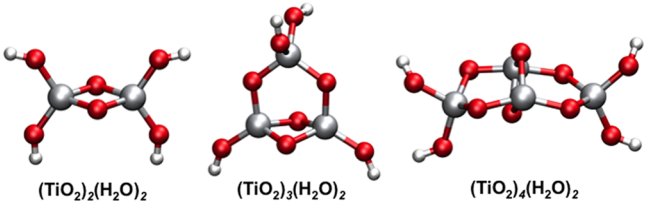

Figure 3. S0 minimum energy geometries for the $(TiO_2)_n(H_2O)_2$ hydrated structures studied. Red spheres denote oxygen atoms, whereas gray and white represent titanium and hydrogen atoms, respectively.

RESULTS AND DISCUSSION

In this section we compare the properties and character of the S1 minima obtained with the different XC potentials, including differences in the predicted photoluminescence signature. For selected TiO_2 nanoparticles, we will focus in detail on the structural and electronic changes associated with the excited state relaxation responsible for the red shift between absorption and photoluminescence. Finally, we will discuss excited state relaxation for hydrated structures.

Photoluminescence and Excited State Relaxation. For each nanoparticle we relaxed the geometry of the lowest singlet excited state (S1) along a downhill path in order to find the S1 excited state minimum energy geometry. We subsequently calculated, for each of the S1 minimum energy geometries, the harmonic frequencies to verify that the found stationary points indeed correspond to minima on the respective S1 potential energy surfaces. Figure 4 shows the trends in the PL energy with particle size for the different XC potentials (see section ESI-3 of the Supporting Information for the same trend in the case of vertical excitations), and Figure 5 shows the trends in the Stokes' shift, the difference between the S1 vertical excitation and PL energy. Table 1, finally, contains the two contributions to the Stokes' shift: the excited state stabilization energy (ESSE) and the ground state destabilization energy (GSDE).

From Figure 5 and Table 1 it is clear that all XC potentials predict that for all nanoparticles, with the exception of $(TiO_2)_1$ studied before by us[26] and others,[20,65,66] the relaxation on the S1 surface is associated with a significant Stokes' shift. This Stokes' shift is the result of both an energetic stabilization of the excited state and a destabilization of the ground state when going from the ground state geometry to the excited state minimum energy geometry. The ESSE and GDSE are as a rule of similar magnitude, where the latter in the case of TD-CAM-B3LYP and TD-BHLYP at least is generally slightly larger than the former. Overall, this picture is very similar to that observed by us previously for ZnS nanoparticles.[39−42]

Comparing the predictions of TD-DFT calculations using the different XC potentials, it appears that the results obtained with TD-CAM-B3LYP and TD-BHLYP are very similar (average difference between predicted PL energies of 10%), whereas those from TD-B3LYP are substantially different

dx.doi.org/10.1021/ct500787x | J. Chem. Theory Comput. XXXX, XXX, XXX−XXX

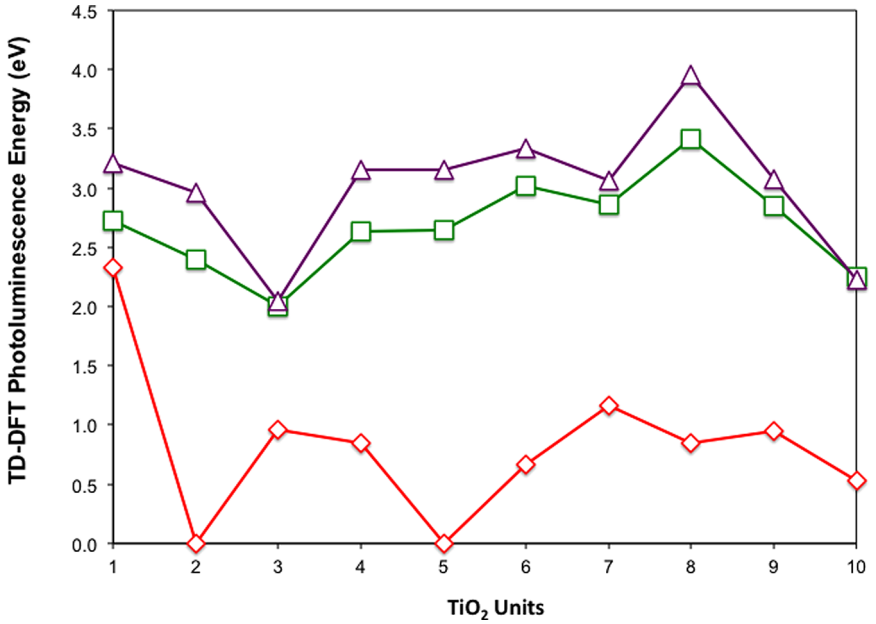

Figure 4. TD-DFT calculated photoluminescence energies for the naked $(TiO_2)_n$ particles: TD-B3LYP (red diamonds), TD-CAM-B3LYP (green squares), and TD-BHLYP (purple triangles). All values are in eV.

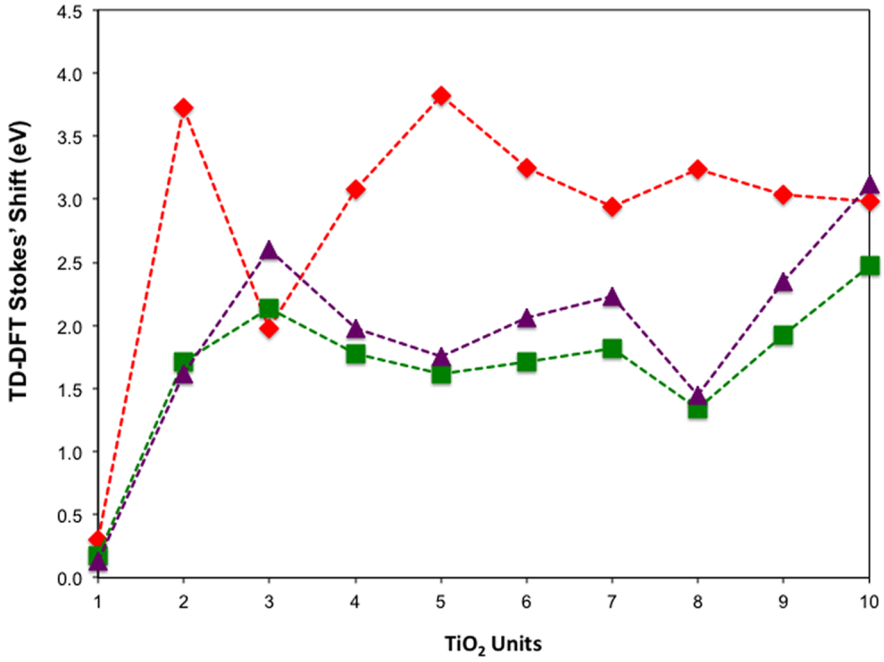

Figure 5. TD-DFT calculated Stokes' shift for the naked $(TiO_2)_n$ particles: TD-B3LYP (red diamonds), TD-CAM-B3LYP (green squares), and TD-BHLYP (purple triangles). All values are in eV.

(average difference of 70%). Just as the case for the vertical excitation energies, the TD-BHLYP PL energies are generally shifted to higher values than their TD-CAM-B3LYP counterparts. The exception are two nanoparticles, $(TiO_2)_3$ and $(TiO_2)_{10}$, for which the TD-BHLYP and TD-CAM-B3LYP PL energies essentially coincide. Figure 5 demonstrates that the latter observation is related to the fact that while the TD-BHLYP and TD-CAM-B3LYP Stokes' shifts are overall very similar, the difference between the predictions of the two XC potentials is the largest for $(TiO_2)_3$ and $(TiO_2)_{10}$. More generally, there appears to be an inverse relationship between the difference in predicted Stokes' shift and the difference in predicted PL energy.

TD-B3LYP predicts, in contrast to TD-CAM-B3LYP and TD-BHLYP, not only much lower PL energies, as could naively have been expected on the basis of what is observed for the vertical excitation energies, but overall also much larger Stokes' shifts. The extent of TD-B3LYP relaxation thus appears to be much larger than that for the other XC potentials, suggesting that the effect of switching XC potential here goes beyond a simple rigid shift and that instead the TD-B3LYP S1 excited state minima are different in structure and/or chemical character than their TD-CAM-B3LYP and TD-BHLYP

dx.doi.org/10.1021/ct500787x | J. Chem. Theory Comput. XXXX, XXX, XXX−XXX

Table 1. Lowest Vertical Excitation Energy (EE), Photoluminescence Energy (PLE), Excited State Stabilization Energy (ESSE), and Ground State Destabilization Energy (GSDE) Values, as Calculated with Different XC-Potentials, for the $(TiO_2)_n$ Particles[a]

	TD-B3LYP				TD-CAMB3LYP				TD-BHLYP			
$(TiO_2)_n$	EE	PLE	ESSE	GSDE	EE	PLE	ESSE	GSDE	EE	PLE	ESSE	GSDE
1	2.64	2.33	0.22	0.09	2.90	2.73	0.06	0.11	3.34	3.21	0.05	0.09
2	3.72	**0.00**	**0.35**	**3.37**	4.11	2.39	0.71	1.00	4.58	2.96	0.75	0.87
3	2.94	0.96	0.93	1.05	4.14	2.00	0.81	1.33	4.65	2.04	1.09	1.51
4	3.92	0.85	1.46	1.62	4.42	2.64	0.71	1.07	5.13	3.16	0.82	1.15
5	3.82	**0.00**	**0.44**	**3.38**	4.25	2.64	0.64	0.97	4.91	3.15	0.69	1.06
6	3.91	0.67	0.74	2.50	4.72	3.02	0.64	1.07	5.39	3.34	0.82	1.24
7	4.10	1.16	1.49	1.45	4.67	2.86	0.77	1.05	5.30	3.06	1.07	1.17
8	4.08	0.85	1.54	1.69	4.76	3.41	0.51	0.83	5.40	3.57	0.56	0.88
9	3.98	0.95	1.50	1.54	4.77	2.84	0.74	1.18	5.42	3.07	1.01	1.35
10	3.51	0.53	2.80	0.18	4.72	2.24	0.87	1.60	5.35	2.23	1.27	1.85

[a]The TD-B3LYP results for both $(TiO_2)_2$ and $(TiO_2)_5$ structures shown in bold correspond to the energies calculated at the conical intersection between S1 and S0. All values are shown in eV.

counterparts. As shown in Figure 4, when employing TD-B3LYP we also predict for two structures, $(TiO_2)_2$ and $(TiO_2)_5$, what appear to be conical intersections, not observed for TD-CAM-B3LYP and TD-BHLYP. EOM-CCSD/def2-SVP S1 relaxation for $(TiO_2)_2$, intractable for larger nanoparticles, yields an excited state minimum energy geometry that is similar in structure and properties to that found for TD-CAM-B3LYP and TD-BHLYP and distinctly different from that obtained with TD-B3LYP (see below). Finally, for two structures, $(TiO_2)_3$ and $(TiO_2)_{10}$, the Stokes' shift predicted by TD-B3LYP is nearly identical to that obtained using TD-CAM-B3LYP and TD-BHLYP. We believe this fit to be completely fortuitous. Moreover, as TD-B3LYP substantially underestimates the vertical excitation energies for these particles and predicts significantly lower PL values than TD-CAM-B3LYP and TD-BHLYP (differences in both cases >1 eV), the successful prediction of Stokes' shift for these two particles is of little or no practical use.

Charge-Transfer Character. In our previous paper we showed that TD-B3LYP struggles to describe vertical excitations of selected nanoparticles due to a spurious stabilization of charge transfer states. We used the Λ diagnostic of Peach and co-workers[53] to probe for such potentially problematic CT states. The Λ diagnostic is a measure of the overlap between the occupied and virtual orbitals involved with an excitation and can range between 0, no overlap, and 1, complete overlap. We found that excitation energies of vertical excitations of TiO_2 particles with a Λ diagnostic of 0.15 or less were severely underestimated.[28]

In order to test if the extended excited state relaxation observed for TD-B3LYP is related to (changes in) the charge-transfer character of the lowest excited state, we calculated the S1 Λ diagnostic for the S1 minimum energy structures (S1/S1). Table 2 compares the S1/S1 Λ diagnostic values with those calculated at the ground state minimum energy geometries (S1/S0). While Λ diagnostic values of all three of the XC potentials are given, we focus on those for TD-B3LYP as previous work showed that only for TD-B3LYP (and GGA XC potentials) there appears to be a clear link between the value of the Λ diagnostic and the likeliness that the description of a particular excitation is problematic due to its CT character.

Table 2 shows that the TD-B3LYP Λ diagnostic decreases to values of 0.17 or lower when going from the ground state to the excited state minimum energy geometry. The exception are the two nanoparticles for which S1 already has a strong CT

Table 2. Λ Diagnostic Values for S1/S0 min (Vertical Excitations) and S1/S1 min (Photoluminescene Energy, PLE) Minimum Energy Structures, as Calculated with TD-B3LYP, TD-CAM-B3LYP, and TD-BHLYP[a]

	S1/S0 min			S1/S1 min		
$(TiO_2)_n$	TD-B3LYP	TD-CAM-B3LYP	TD-BHLYP	TD-B3LYP	TD-CAM-B3LYP	TD-BHLYP
1	0.26	0.26	0.25	0.24	0.26	0.25
2	0.30	0.29	0.28	(0.10)	0.20	0.22
3	0.10	0.18	0.10	0.15	0.13	0.12
4	0.22	0.27	0.27	0.17	0.24	0.26
5	0.24	0.24	0.23	(0.11)	0.23	0.22
6	0.25	0.31	0.30	0.13	0.29	0.27
7	0.19	0.32	0.29	0.15	0.27	0.24
8	0.24	0.33	0.33	0.14	0.29	0.36
9	0.19	0.29	0.28	0.13	0.32	0.31
10	0.08	0.27	0.22	0.10	0.16	0.16

[a]For all the nanoparticles studied only the lowest energy excited state minimum is shown in this table. The two values shown in brackets correspond to the structures for which we observed a CX between S1 and S0. The Λ diagnostic values are dimensionless numbers.

character at the ground state minimum energy geometry, $(TiO_2)_3$ and $(TiO_2)_{10}$, in which cases the Λ diagnostic values are found to slightly increase, and the monomer, for which the Λ diagnostic value stays approximately constant. For most particles, the CT character of the S1 states thus increases during excited state relaxation. Moreover, after relaxation, the S1 Λ diagnostic value is now in almost all cases suggestive of potential problems in describing this state with TD-B3LYP due to its CT character ($\Lambda \leq 0.15$).

These low Λ diagnostic values are probably part of the origin of the large discrepancy between the predictions of TD-B3LYP and those obtained with TD-CAM-B3LYP and TD-BHLYP observed above. Another, more perverse, related reason might be that CT states are spuriously stabilized by TD-B3LYP and that there is thus a fictitious energetic driving force during energy minimization for a state, where possible, to increase its CT character. While it is hard to unequivocally demonstrate that this is happening for any of the TiO_2 nanoparticles, it is in line with the observation that for almost all particles the S1 Λ diagnostic value decreases in the case of TD-B3LYP during excited state relaxation. S1 Λ diagnostic values for other XC potentials than TD-B3LYP indeed show in contrast a small

dx.doi.org/10.1021/ct500787x | J. Chem. Theory Comput. XXXX, XXX, XXX−XXX

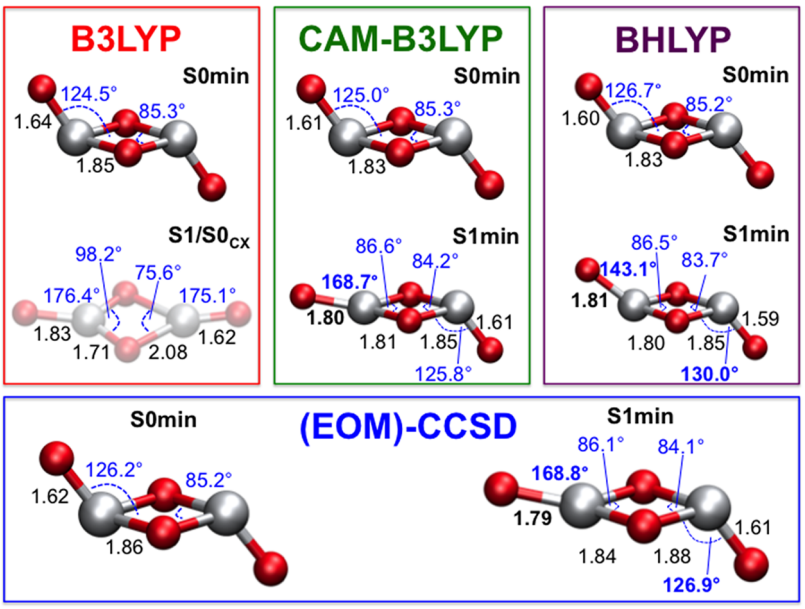

Figure 6. Comparison of the geometries of the ground (S0) and lowest excited state (S1) minimum energy structures for the tentative $(TiO_2)_2$ GM structure obtained with the different method combinations. The TD-B3LYP S1/S0 CX structure is shown semitransparent.

increase (e.g., $(TiO_2)_9$) or only a very minor decrease upon excited state relaxation for selected nanoparticles. Moreover, something very similar was observed in the case of an organic system (4-(dimethylamino)benzonitrile),[67] where problems with describing CT excitations also appear to drive the structure, in the case of low-HFLE XC potentials, toward a spurious excited state minimum with a low Λ diagnostic value, which is furthermore structurally dramatically different from that found with TD-CAM-B3LYP and approximate coupled cluster theory.

(Electronic) Structure of the Predicted S1 Minima. Having discussed overall trends in PL energy, Stokes' shift, and CT character, we will now focus on the (TD-)DFT predictions for three specific nanoparticles: $(TiO_2)_2$, $(TiO_2)_3$, and $(TiO_2)_6$. These structures were specifically chosen as they represent interesting cases where the use of the different XC potentials results in different predictions for the properties of the vertical and/or relaxed excited states.

$(TiO_2)_2$. As discussed above, TD-B3LYP predicts what appears to be a conical intersection between S0 and S1 for $(TiO_2)_2$, while in the case of TD-CAM-B3LYP and TD-BHLYP S1 minima were obtained with photoluminescence energies of 2.39 and 2.96 eV, respectively. Figure 6 compares the S0 and S1 minimum energy structures obtained with the different XC potentials and EOM-CCSD. All method combinations predict very similar C_{2h} S0 minima but make rather different predictions for the S1 minimum energy structures (even if the final symmetry is C_s in all cases).

In the case of TD-CAM-B3LYP, TD-BHLYP, and EOM-CCSD the symmetry lowering to C_s is associated with an elongation of one of the two terminal Ti−O bonds and a flattening of the angle between the terminal oxygen atom in this Ti−O bond and the main Ti_2O_2 plane of the particle (i.e., the O−Ti−Ti angle). Figure 7, which displays the density difference between S0 and S1 for the S0 and S1 minimum energy geometries for (TD-)B3LYP and (TD-)BHLYP, shows that in the case of TD-BHLYP this structural distortion is associated with a localization of the hole and excited electron component of the excited state on the same side of the particle.

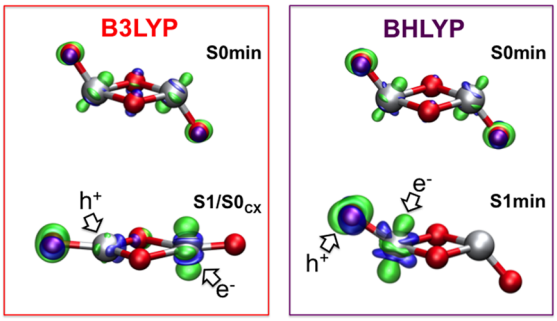

Figure 7. TD-B3LYP and TD-BHLYP excited state density difference plots obtained for the vertical (S0/S0 min) and PL (S1/S1 min) excitations of the $(TiO_2)_2$ GM structure. The isodensity plots for the excited state density are calculated at a value of 0.02 au, where the green lobes represent regions of excess electron density (where the excited electron component of the excited state is located, e^-), whereas the blue lobes represent regions deficient in electron density (where the hole component is found, h^+).

The structure of the rest of the nanoparticle stays relatively unchanged compared to the structure of the ground state minimum energy geometry.

The structure of the TD-B3LYP S0/S1 conical intersection is very different from the S1 minimum energy geometries found by the other method combinations. After S1 excited state relaxation the structure of the whole particle is flattened. One of the terminal Ti−O bonds elongates to 1.83 Å, and its O−Ti−Ti angle reaches approximately 176°. The length of the other terminal Ti−O bond stays roughly unchanged, while its O−Ti−Ti angle also increases from 124.5° in the ground state to approximately 175°. In line with this rather different S1 structure, Figure 7 shows that in the TD-B3LYP S0/S1 CX-structure the electron and hole components are localized on opposite sides of the nanoparticle instead of on the same side, as seen for TD-BHLYP. It also explains the much larger CT character and rather low S1 TD-B3LYP Λ diagnostic value. Finally, the slightly larger elongation of the terminal Ti−O bond in the case of TD-B3LYP, relative to that seen by the

dx.doi.org/10.1021/ct500787x | J. Chem. Theory Comput. XXXX, XXX, XXX−XXX

other method combinations, is probably due to the fact that in the TD-B3LYP case the δ^+ (hole component of the excited state) charge does not sit on the titanium atom of the elongated terminal Ti−O bond.

A similar analysis can be performed for the $(TiO_2)_5$ nanoparticle, which corresponds to the other case where TD-B3LYP predicts a CX between the S0 and S1 surfaces. A detailed discussion for this structure can be found in the Supporting Information (section ESI-4).

$(TiO_2)_3$. In our previous work we found that the vertical S1 excitation at the ground state geometry of $(TiO_2)_3$ had strong CT character for all XC potentials considered. After excited state relaxation, we find here, as discussed above, for all XC potentials stable S1 minima with similar Stokes' shifts of ∼2 eV. In line with these observations, Figure 8 shows that the S0/S1

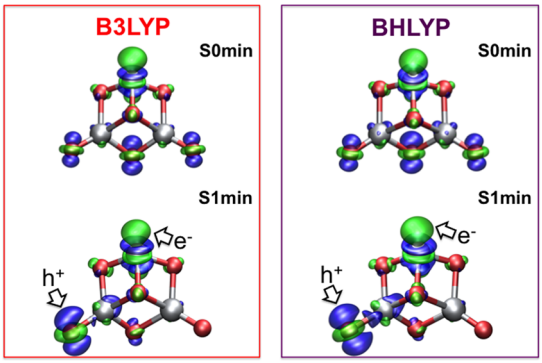

Figure 8. TD-B3LYP and TD-BHLYP excited state density difference plots obtained for the vertical (S0/S0 min) and PL (S1/S1 min) excitations of the $(TiO_2)_3$ GM structure. The isodensity plots for the excited state density are calculated at a value of 0.02 au, where the green lobes represent regions of excess electron density (where the excited electron component of the excited state is located, e^-), whereas the blue lobes represent regions deficient in electron density (where the hole component is found, h^+).

density difference for the ground state minimum energy geometry is very similar for both TD-B3LYP and TD-BHLYP and that the same holds for the S1 excited state minimum energy geometry. Both for the ground and excited state geometries, the density difference clearly shows that the S1 state is a CT state, involving both the 3-coordinated titanium atom (excited electron component of the excited state) and the two terminal oxygen atoms (hole component of the excited state). The excited state relaxation is associated with a localization of the hole component of the excited state on one of the two terminal oxygen atoms. Figure 8 shows that this localization is associated with an asymmetric distortion of the nanoparticle structure, including an elongation of 0.2 Å of the Ti−O bond involving the terminal oxygen atom on which the hole becomes localized.

$(TiO_2)_6$. If the two structures for which we found the CXs are ignored, then $(TiO_2)_6$ is the nanoparticle with the largest difference between the PL energy predicted by TD-B3LYP and that obtained with TD-CAM-B3LYP and TD-BHLYP. For TD-B3LYP, the S1 Λ diagnostic value also decreases strongly moving from the S1/S0 to the S1/S1 geometry but shows only a slight reduction for TD-CAM-B3LYP and TD-BHLYP. It is, therefore, not surprising that Figure 9 shows that density differences for both the ground and excited state minimum energy structures are completely different for TD-B3LYP and

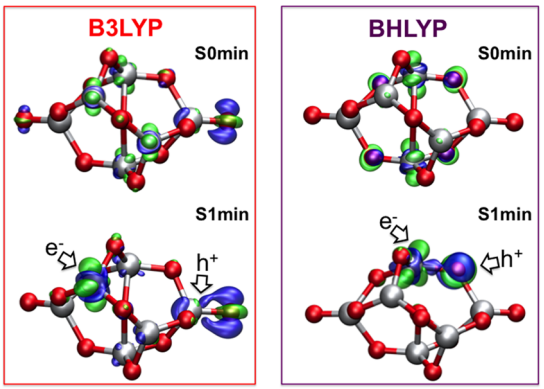

Figure 9. TD-B3LYP and TD-BHLYP excited state density difference plots obtained for the vertical (S0/S0 min) and PL (S1/S1 min) excitations of the $(TiO_2)_6$ GM structure. The isodensity plots for the excited state density are calculated at a value of 0.02 au, where the green lobes represent regions of excess electron density (where the excited electron component of the excited state is located, e^-), whereas the blue lobes represent regions deficient in electron density (where the hole component is found, h^+).

TD-BHLYP. For example, the hole component of the TD-B3LYP excited state involves one of the two terminal oxygen atoms, whereas for TD-BHLYP both the hole and excited electron components of the excited state are localized on the center of the nanoparticle. The relaxed structures shown in Figure 9 are, as a result, also substantially different. A similar analysis can be carried out for the $(TiO_2)_8$ nanoparticle, and its discussion is included in the section ESI-5 of the Supporting Information.

Hydrated Particles. Finally, we consider excited state relaxation in the case of hydrated structures. In our previous work[28] we found that TD-B3LYP in general appears to predict reasonable vertical excitation energies for hydrated systems. We believe this is due to the fact that hydration increases the coordination of the undercoordinated atoms, e.g. terminal oxygen atoms, that otherwise give rise to CT states (see section ESI-6 of the Supporting Information).

While the description of vertical excitations is non-problematic with TD-B3LYP, the same does not appear to be necessarily true in the case of excited state relaxation. In particular, as shown in Figure 10 and Figure 11, for the $n = 2$ nanoparticle the PL energy is far lower as calculated with TD-B3LYP than with TD-CAM-B3LYP and TD-BHLYP. This is not the case for the other two hydrated particles, where TD-DFT calculations with all XC potentials make similar predictions. For the former particle, TD-B3LYP predicts a much lower photoluminescence energy than TD-CAM-B3LYP and TD-BHLYP. Similarly, the TD-B3LYP S1 Λ diagnostic values for $(TiO_2)_3(H_2O)_2$ and $(TiO_2)_4(H_2O)_2$ do not change much between the S0 and S1 minimum energy geometries, whereas the $(TiO_2)_2(H_2O)_2$ TD-B3LYP S1 Λ diagnostic value plummets (see Table 3). Using TD-B3LYP we predict that during excited state relaxation the character of the S1 state of $(TiO_2)_2(H_2O)_2$ changes from a non-CT state to a CT state. The S1 character of the same particle with the other XC potentials as well as that for the other hydrated particles, in contrast, appears to not substantially change.

The density difference plots for the $(TiO_2)_2(H_2O)_2$ particle shown in Figure 12, and those for the $(TiO_2)_3(H_2O)_2$ and $(TiO_2)_4(H_2O)_2$ structures in the Supporting Information (ESI-7 and ESI-8) support the observations above. Specifically, for

dx.doi.org/10.1021/ct500787x | J. Chem. Theory Comput. XXXX, XXX, XXX−XXX

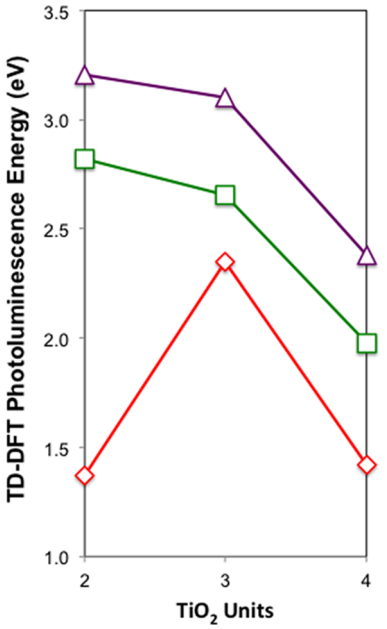

Figure 10. TD-DFT calculated photoluminescence energies for the hydrated particles: TD-B3LYP (red diamonds), TD-CAM-B3LYP (green squares), and TD-BHLYP (purple triangles). All values are in eV.

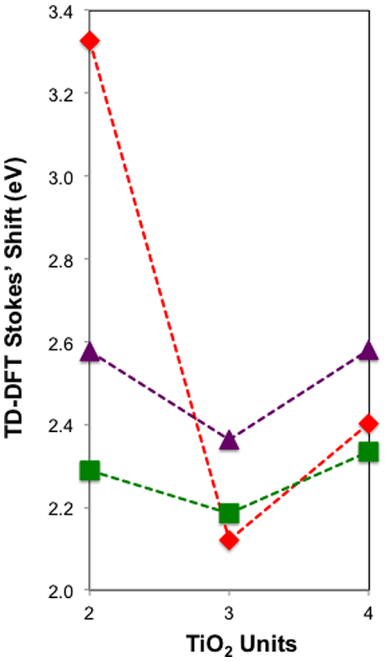

Figure 11. TD-DFT calculated Stokes' shift for the hydrated particles: TD-B3LYP (red diamonds), TD-CAM-B3LYP (green squares), and TD-BHLYP (purple triangles). All values are in eV.

the $(TiO_2)_2(H_2O)_2$ particle, the use of TD-B3LYP and TD-BHLYP yields similar density differences for the ground state geometry but rather different density differences in the case of the S1 minimum energy structures. TD-B3LYP predicts an excited state minimum structure where the hole-component of the excited state is localized on the oxygen of one of the hydroxyl groups and the excited electron component on the titanium atom furthest away from this hydroxyl. In line with the discussion above, this is a clear CT state. TD-BHLYP, in contrast, finds an excited state minimum where, just as in the ground state geometry, both the hole and excited electron component of the excited state are localized on the center of the nanoparticle and in which the hydroxyl groups do not partake.

The example of the $(TiO_2)_2(H_2O)_2$ particle suggests that even if the use of TD-B3LYP for vertical excitations is nonproblematic, one cannot guarantee that the same would also be the case when describing excited state relaxation. Moreover, the apparent change of a non-CT into a CT state suggests that this might perhaps be another example of the spurious stabilization of CT states driving a state to increase its CT character.

Concentrating on the TD-CAM-B3LYP and TD-BHLYP results, we see that, just as was the case of the naked particles, excited state relaxation for the small hydrated particles is associated with a rather large Stokes' shift of 2−3 eV. Also, just as for the naked particles, the contribution of ground state distortion and excited state stabilization to the Stokes' shift are both significant.

Discussion. From our results, it is clear that TD-B3LYP predicts considerably different PL energies, Stokes' shifts, chemical character, and geometries for the S1 minima of $(TiO_2)_n$ nanoparticles than TD-CAM-B3LYP and TD-BHLYP. We can only compare directly with CC theory for $(TiO_2)_2$, where TD-CAM-B3LYP and TD-BHLYP find a stable minimum with PL energies and Stokes' shifts that quantitatively fit with those obtained with EOM-CCSD, whereas TD-B3LYP predicts instead an apparent S0/S1 conical intersection. Moreover, the fact that use of TD-B3LYP results in almost all cases in Λ diagnostic values of 0.15 or less for the S1 minima/conical intersection structures obtained strongly suggests that the problem lies with TD-B3LYP. Where TD-B3LYP gives reasonable results for vertical excitations at ground state geometries for most nanoparticles and fails dramatically only in selected cases, the problem with excited state relaxation appears much more widespread, and TD-B3LYP results are likely to be severely wrong for any naked TiO_2 particle. Moreover, analogous problems are likely to occur when using GGA XC potentials or hybrid XC potentials with a similar or smaller amount of HFLE as B3LYP (e.g., PBE0).

Description of excited states for hydrated particles, nonproblematic and unambiguous in the case of vertical excitations as all XC potentials give similar results, appears also to become problematic when going beyond the ground state geometry. As discussed above, for selected particles, TD-B3LYP finds a S1 minimum with clear CT character, whereas use of any of the other XC potentials yields non-CT S1 minima. We lack CC benchmark data for the hydrated particles but as the origin of the discrepancy between TD-B3LYP and TD-CAM-B3LYP/TD-BHLYP is similar as in the case of the naked particles, we believe that it is likely that the problem again lies with TD-B3LYP. Again, we expect that similar problems are likely to occur when using GGA XC potentials or hybrid XC potentials with a low percentage of HFLE to describe excited state relaxation in hydrated titania particles.

For many particles, the character of S1 changes from a local excitation to a CT state after excited state relaxation when using TD-B3LYP, whereas the character of the excited state does not change when using TD-CAM-B3LYP and TD-BHLYP. We conclude that the spurious energetic stabilization of CT states in TD-B3LYP in effect may result in a fictitious driving force toward minima with a strong CT character.

dx.doi.org/10.1021/ct500787x | J. Chem. Theory Comput. XXXX, XXX, XXX−XXX

Table 3. Vertical Excitation Energies (EE), Photoluminescence (PLE) and Corresponding Λ Diagnostic Values, as Calculated with TD-B3LYP, TD-CAM-B3LYP, and TD-BHLYP, for the Hydrated Particles[a]

	TD-B3LYP				TD-CAMB3LYP				TD-BHLYP			
$(TiO_2)_n(H_2O)_2$	EE	EE Λ	PLE	PLE Λ	EE	EE Λ	PLE	PLE Λ	EE	EE Λ	PLE	PLE Λ
2	4.70	0.30	1.37	0.10	5.11	0.31	2.82	0.37	5.78	0.31	3.21	0.37
3	4.47	0.31	2.35	0.37	4.84	0.31	2.65	0.37	5.47	0.31	3.10	0.35
4	3.82	0.32	1.42	0.32	4.31	0.32	1.98	0.36	4.96	0.30	2.38	0.38

[a]For all the nanoparticles studied only the lowest energy excited state minimum is shown in this table. EE and PLE values are shown in eV, whereas the Λ diagnostic values are dimensionless numbers.

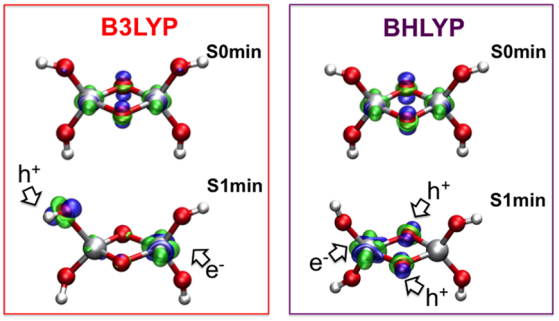

Figure 12. TD-B3LYP and TD-BHLYP excited state density difference plots obtained for the vertical (S0/S0 min) and PL (S1/S1 min) excitations of the $(TiO_2)_2(H_2O)_2$ particle. The isodensity plots for the excited state density are calculated at a value of 0.01 au, where the green lobes represent regions of excess electron density (where the excited electron component of the excited state is located, e^-), whereas the blue lobes represent regions deficient in electron density (where the hole component is found, h^+).

Based on the qualitative fit with EOM-CCSD, both in terms of PL energy for $(TiO_2)_2$ and vertical excitations for $(TiO_2)_2$ to $(TiO_2)_6$ and selected hydrated particles, TD-CAM-B3LYP should be preferred over TD-BHLYP for excited state properties, also because CAM-B3LYP is known to well reproduce other nonexcited state properties.[52] However, in the absence of CAM-B3LYP or range-separated XC potentials in general, BHLYP appears to be a good alternative, possibly in combination with a posterior rigid red-shift of the predicted excitation energies.

Focusing on the TD-CAM-B3LYP and TD-BHLYP results, there is a clear variation from particle to particle in the predicted Stokes' shift and photoluminescence energy. This variation probably finds its origin in the different sites that the excited electron and hole components of the excited state localize upon in the different structures. Just as we previously hypothesized in the case of vertical excitations,[28] the latter is probably the result of a subtle interplay between the on-site electrostatic potential and the electrostatic interaction between electron and hole. However, in the case of excited state relaxation, there is probably an additional contributing factor; differences in ionic polarizability between different sites in the (different) particle(s). The degree to which different sites allow stabilization of the excited electron and hole components of the excited state by structural distortion, e.g. the elongation of the titanium−terminal oxygen bond upon localization of the hole component on the terminal oxygen atom. Finally, a similar subtle interplay is probably the reason why one encounters CT problems for some hydrated particles and not for other very similar hydrated particles.

CONCLUSION

In this paper we have investigated the description of excited state relaxation in TiO_2 nanoparticles by (TD-)DFT. We considered three common exchange-correlation potentials—B3LYP, CAM-B3LYP, and BHLYP—and particles ranging in size from $(TiO_2)_2$ to $(TiO_2)_{10}$. We find that use of TD-CAM-B3LYP and TD-BHLYP yields qualitatively similar results for all structures, which are furthermore consistent with predictions of EOM-CCSD for $(TiO_2)_2$. TD-B3LYP, in contrast, is found to make rather different predictions, including an apparent conical intersection for $(TiO_2)_2$ that is not observed for higher quality calculations. In line with what we previously observed for vertical excitations, the issue with TD-B3LYP appears to be its inherent tendency to spuriously stabilize the energy of charge-transfer states. Even for hydrated particles, for which vertical excitations are generally well described with all exchange-correlation potentials, use of TD-B3LYP appears to result in charge-transfer problems during excited state relaxation for some specific particles. This spurious stabilization drives TD-B3LYP excited state optimizations to different structures than those obtained using TD-CAM-B3LYP or TD-BHLYP. On the basis of these observations, we recommend the use of CAM-B3LYP, BHLYP, or similar exchange-correlation potentials when describing processes taking place on the excited state potential energy surfaces of TiO_2 nanostructures. Finally, focusing on the TD-CAM-B3LYP and TD-BHLYP results, excited state relaxation in small naked and hydrated TiO_2 nanoparticles is predicted to be associated with a large Stokes' shift. The exact magnitude of the Stokes' shift and PL energy depends on the sites on which the excited electron and hole components of the excited state localize upon.

ASSOCIATED CONTENT

Supporting Information

Optimized excited state geometries of all the naked and hydrated $(TiO_2)_n$ nanoparticles obtained using TD-DFT (B3LYP, CAM-B3LYP, and BHLYP) and the def2-TZVP basis set; trends in the TD-DFT lowest vertical excitation energies for the naked and hydrated $(TiO_2)_n$ particles optimized in the ground state with different XC potentials; comparison between the geometries and the excited state density difference plots obtained for the vertical (S0/S0 min) and PL ($S1/S0_{CX}$ and S1/S1 min) excitations for the $(TiO_2)_5$, $(TiO_2)_8$ GM structure and for the $(TiO_2)_3(H_2O)_2$ and $(TiO_2)_4(H_2O)_2$ hydrated particles. This material is available free of charge via the Internet at http://pubs.acs.org.

AUTHOR INFORMATION

Corresponding Author

*E-mail: m.zwijnenburg@ucl.ac.uk.

dx.doi.org/10.1021/ct500787x | J. Chem. Theory Comput. XXXX, XXX, XXX−XXX

Notes

The authors declare no competing financial interest.

■ ACKNOWLEDGMENTS

We kindly acknowledge Prof. S. Bromley, Prof. F. Illas, Prof. A. Shluger, Prof. F. Furche, Dr. M. Calatayud, and Dr. A. A. Sokol for stimulating discussions. M.A.Z. acknowledges the UK Engineering and Physical Sciences Research Council (EPSRC) for a Career Acceleration Fellowship (Grant EP/I004424/1). This study has further been supported by a UCL Impact studentship award to E.B. Computational time on the computers of the Unity High Performance Computing Facility at University College London, the IRIDIS regional high-performance computing service provided by the e-Infrastructure South Centre for Innovation (EPSRC Grants EP/K000144/1 and EP/K000136/1), and on Archer the UK's national high-performance computing service (via our membership of the UK's HPC Materials Chemistry Consortium, which is funded by EPSRC grant EP/L000202/1) is gratefully acknowledged. A significant portion of the research was also performed using PNNL Institutional Computing at Pacific Northwest National Laboratory and EMSL, a national scientific user facility sponsored by the Department of Energy's Office of Biological and Environmental Research and located at Pacific Northwest National Laboratory. The Pacific Northwest National Laboratory is operated for the U.S. Department of Energy by the Battelle Memorial Institute under Contract DEAC06.76RLO-1830.

■ REFERENCES

(1) Fujishima, A.; Honda, K. Electrochemical photolysis of water at a semiconductor electrode. *Nature* **1972**, *238*, 37−38.
(2) Schrauzer, G. N.; Guth, T. D. Photolysis of water and photoreduction of nitrogen on titanium dioxide. *J. Am. Chem. Soc.* **1977**, *99*, 7189−7193.
(3) Satoh, N.; Nakashima, T.; Kamikura, K.; Yamamoto, K. Quantum size effect in TiO_2 nanoparticles prepared by finely controlled metal assembly on dendrimer templates. *Nat. Nanotechnology* **2008**, *3*, 106−111.
(4) Maeda, K.; Domen, K. Photocatalytic Water Splitting: Recent Progress and Future Challenges. *J. Chem. Phys. Lett.* **2010**, *1*, 2655−2661.
(5) Henderson, M. A. A surface science perspective on TiO_2 photocatalysis. *Surf. Sci. Rep.* **2011**, *66*, 185−297.
(6) Hisatomi, T.; Kubota, J.; Domen, K. Recent advances in semiconductors for photocatalytic and photoelectrochemical water splitting. *Chem. Soc. Rev.* **2014**, *43*, , 7520−7535.
(7) Oregan, B.; Gratzel, M. A low-cost, high-efficiency solar-cell based on dye-sensitized colloidal TiO_2 films. *Nature* **1991**, *353*, 737−740.
(8) Gratzel, M. Recent Advances in Sensitized Mesoscopic Solar Cells. *Acc. Chem. Res.* **2009**, *42*, 1788−1798.
(9) Ohno, T.; Sarukawa, K.; Matsumura, M. Photocatalytic activities of pure rutile particles isolated from TiO_2 powder by dissolving the anatase component in HF solution. *J. Phys. Chem. B* **2001**, *105*, 2417−2420.
(10) Ohno, T.; Sarukawa, K.; Matsumura, M. Crystal faces of rutile and anatase TiO_2 particles and their roles in photocatalytic reactions. *New J. Chem.* **2002**, *26*, 1167−1170.
(11) Cho, C. H.; Han, M. H.; Kim, D. H.; Kim, D. K. Morphology evolution of anatase TiO_2 nanocrystals under a hydrothermal condition (pH = 9.5) and their ultra-high photo-catalytic activity. *Mater. Chem. Phys.* **2005**, *92*, 104−111.
(12) Amano, F.; Prieto-Mahaney, O.-O.; Terada, Y.; Yasumoto, T.; Shibayama, T.; Ohtani, B. Decahedral Single-Crystalline Particles of Anatase Titanium (IV) Oxide with High Photocatalytic Activity. *Chem. Mater.* **2009**, *21*, 2601−2603.
(13) Murakami, N.; Kurihara, Y.; Tsubota, T.; Ohno, T. Shape-Controlled Anatase Titanium (IV) Oxide Particles Prepared by Hydrothermal Treatment of Peroxo Titanic Acid in the Presence of Polyvinyl Alcohol. *J. Phys. Chem. C* **2009**, *113*, 3062−3069.
(14) Cernuto, G.; Masciocchi, N.; Cervellino, A.; Colonna, G. M.; Guagliardi, A. Size and shape sependence of the photocatalytic activity of TiO_2 nanocrystals: a total scattering debye function study. *J. Am. Chem. Soc.* **2011**, *133*, 3114−3119.
(15) Li, Y.-F.; Liu, Z.-P. Particle size, shape and activity for photocatalysis on titania anatase nanoparticles in aqueous surroundings. *J. Am. Chem. Soc.* **2011**, *133*, 15743−15752.
(16) Nunzi, F.; Storchi, L.; Manca, M.; Giannuzzi, R.; Gigli, G.; De Angelis, F. Shape and Morphology Effects on the Electronic Structure of TiO_2 Nanostructures: From Nanocrystals to Nanorods. *ACS Appl. Mater. Interfaces* **2014**, *6*, 2468−2475.
(17) Rocca, D.; Gebauer, R.; De Angelis, F.; Nazeeruddin, M. K.; Baroni, S. Time-dependent density functional theory study of squaraine dye-sensitized solar cells. *Chem. Phys. Lett.* **2009**, *475*, 49−53.
(18) Blagojevic, V.; Chen, Y. R.; Steigerwald, M.; Brus, L.; Friesner, R. A. Quantum chemical investigation of cluster models for TiO_2 nanoparticles with water-derived ligand passivation: Studies of excess electron states and implications for charge transport in the Gratzel cell. *J. Phys. Chem. C* **2009**, *113*, 19806−19811.
(19) Shevlin, S. A.; Woodley, S. M. Electronic and Optical Properties of Doped and Undoped $(TiO_2)_n$ Nanoparticles. *J. Phys. Chem. C* **2010**, *114*, 17333−17343.
(20) Taylor, D. J.; Paterson, M. J. Calculations of the low-lying excited states of the TiO_2 molecule. *J. Chem. Phys.* **2010**, *133*, 204302.
(21) De Angelis, F.; Fantacci, S.; Gebauer, R. Simulating Dye-Sensitized TiO_2 Heterointerfaces in Explicit Solvent: Absorption Spectra, Energy Levels, and Dye Desorption. *J. Phys. Chem. Lett.* **2011**, *2*, 813−817.
(22) Chiodo, L.; Salazar, M.; Romero, A. H.; Laricchia, S.; Della Sala, F.; Rubio, A. Structure, electronic, and optical properties of TiO_2 atomic clusters: an ab initio study. *J. Chem. Phys.* **2011**, *135*, 244704−244704.
(23) Auvinen, S.; Alatalo, M.; Haario, H.; Jalava, J. P.; Lamminmäki, R. J. Size and shape dependence of the electronic and spectral properties in TiO_2 nanoparticles. *J. Phys. Chem. C* **2011**, *115*, 8484−8493.
(24) Li, J.; Wang, H.; Persson, P.; Thoss, M. Photoinduced electron transfer processes in dye-semiconductor systems with different spacer groups. *J. Chem. Phys.* **2012**, *137*, 22A529.
(25) Galynska, M.; Persson, P. Emerging Polymorphism in Nanostructured TiO_2: Quantum Chemical Comparison of Anatase, Rutile, and Brookite Clusters. *Int. J. Quantum Chem.* **2013**, *113*, 2611−2620.
(26) Berardo, E.; Hu, H. S.; Kowalski, K.; Zwijnenburg, M. A. Coupled cluster calculations on TiO_2 nanoclusters. *J. Chem. Phys.* **2013**, *139*, 64313.
(27) Hsueh, H. C.; Guo, G. Y.; Louie, S. G. In *Silicon-Based Nanomaterials*; Li, H., Wu, J., Wang, Z. M., Eds.; 2013; Vol. *187*, pp 139−159.
(28) Berardo, E.; Hu, H. S.; Shevlin, S. A.; Woodley, S. M.; Kowalski, K.; Zwijnenburg, M. A. Modeling Excited States in TiO_2 Nanoparticles: On the Accuracy of a TD-DFT Based Description. *J. Chem. Theory Comput.* **2014**, *10*, 1189−1199.
(29) Castelli, I. E.; Landis, D. D.; Thygesen, K. S.; Dahl, S.; Chorkendorff, I.; Jaramillo, T. F.; Jacobsen, K. W. New cubic perovskites for one- and two-photon water splitting using the computational materials repository. *Energy Environ. Sci.* **2012**, *5*, 9034−9043.
(30) Wu, Y.; Lazic, P.; Hautier, G.; Persson, K.; Ceder, G. First principles high throughput screening of oxynitrides for water-splitting photocatalysts. *Energy Environ. Sci.* **2013**, *6*, 157−168.

(31) Guiglion, P.; Butchosa, C.; Zwijnenburg, M. A. Polymeric watersplitting photocatalysts; a computational perspective on the water oxidation conundrum. *J. Mater. Chem. A* **2014**, *2*, 11996−12004.
(32) Stevanovic, V.; Lany, S.; Ginley, D. S.; Tumas, W.; Zunger, A. Assessing capability of semiconductors to split water using ionization potentials and electron affinities only. *Phys. Chem. Chem. Phys.* **2014**, *16*, 3706−3714.
(33) Mom, R. V.; Cheng, J.; Koper, M. T. M.; Sprik, M. Modeling the Oxygen Evolution Reaction on Metal Oxides: The Infuence of Unrestricted DFT Calculations. *J. Phys. Chem. C* **2014**, *118*, 4095−4102.
(34) Sundholm, D. Density functional studies of the luminescence of $Si_{29}H_{36}$. *Phys. Chem. Chem. Phys.* **2004**, *6*, 2044−2047.
(35) Wang, X.; Zhang, R. Q.; Lee, S. T.; Frauenheim, T.; Niehaus, T. A. Anomalous size dependence of the luminescence in reconstructed silicon nanoparticles. *Appl. Phys. Lett.* **2008**, *93*, 243120.
(36) Wang, Y.; Zhang, R.; Frauenheim, T.; Niehaus, T. A. Atomistic Simulations of Self-Trapped Exciton Formation in Silicon Nanostructures: The Transition from Quantum Dots to Nanowires. *J. Phys. Chem. C* **2009**, *113*, 12935.
(37) Zwijnenburg, M. A.; Sokol, A. A.; Sousa, C.; Bromley, S. T. The effect of local environment on photoluminescence: A time-dependent density functional theory study of silanone groups on the surface of silica nanostructures. *J. Chem. Phys.* **2009**, *131*, 34705.
(38) Zwijnenburg, M. A. Optical excitations in stoichiometric uncapped ZnS nanostructures. *Nanoscale* **2011**, *3*, 3780−3787.
(39) Zwijnenburg, M. A.; Illas, F.; Bromley, S. T. The fate of optical excitations in small hydrated ZnS clusters: a theoretical study into the effect of hydration on the excitation and localisation of electrons in Zn_4S_4 and Zn_6S_6. *Phys. Chem. Chem. Phys.* **2011**, *13*, 9311−9317.
(40) Zwijnenburg, M. A.; Sousa, C.; Illas, F.; Bromley, S. T. The fate of optical excitations in small polyhedral ZnS clusters: A theoretical study of the excitation and localization of electrons in Zn_4S_4 and Zn_6S_6. *J. Chem. Phys.* **2011**, *134*, 64511.
(41) Zwijnenburg, M. A. Photoluminescence in semiconductor nanoparticles: an atomistic view of excited state relaxation in nanosized ZnS. *Nanoscale* **2012**, *4*, 3711−3717.
(42) Zwijnenburg, M. A. Excited state localisation cascades in inorganic semiconductor nanoparticles. *Phys. Chem. Chem. Phys.* **2013**, *15*, 11119−11127.
(43) Zhang, R.-Q.; De Sarkar, A.; Niehaus, T. A.; Frauenheim, T. Excited state properties of Si quantum dots. *Phys. Status Solidi B* **2012**, *249*, 401−412.
(44) Hamad, S.; Catlow, C. R. A.; Woodley, S. M.; Lago, S.; Mejias, J. A. Structure and stability of small TiO_2 nanoparticles. *J. Phys. Chem. B* **2005**, *109*, 15741−15748.
(45) Qu, Z. W.; Kroes, G. J. Theoretical study of the electronic structure and stability of titanium dioxide clusters $(TiO_2)_n$ with n = 1−9. *J. Phys. Chem. B* **2006**, *110*, 8998−9007.
(46) Calatayud, M.; Maldonado, L.; Minot, C. Reactivity of $(TiO_2)_n$ Clusters (n = 1−10): Probing Gas-Phase Acidity and Basicity Properties. *J. Phys. Chem. C* **2008**, *112*, 16087−16095.
(47) Syzgantseva, O. A.; Gonzalez-Navarrete, P.; Calatayud, M.; Bromley, S.; Minot, C. Theoretical Investigation of the Hydrogenation of $(TiO_2)_n$ Clusters (n = 1−10). *J. Phys. Chem. C* **2011**, *115*, 15890−15899.
(48) Marom, N.; Kim, M.; Chelikowsky, J. R. Structure selection based on high vertical electron affinity for TiO_2 clusters. *Phys. Rev. Lett.* **2012**, *108*, 106801−106801.
(49) Chen, M.; Dixon, D. A. Tree growth - Hybrid genetic algorithm for predicting the structure of small $(TiO_2)_n$, n = 2−13, nanoclusters. *J. Chem. Theory Comput.* **2013**, *9*, 3189−3200.
(50) Perdew, J. P.; Burke, K.; Ernzerhof, M. Generalized gradient approximation made simple. *Phys. Rev. Lett.* **1996**, *77*, 3865−3868.
(51) Becke, A. D. Density-functional thermochemistry. 3. The role of exact exchange. *J. Chem. Phys.* **1993**, *98*, 5648−5652.
(52) Yanai, T.; Tew, D. P.; Handy, N. C. A new hybrid exchange-correlation functional using the Coulomb-attenuating method (CAM-B3LYP). *Chem. Phys. Lett.* **2004**, *393*, 51−57.
(53) Peach, M. J. G.; Benfield, P.; Helgaker, T.; Tozer, D. J. Excitation energies in density functional theory: An evaluation and a diagnostic test. *J. Chem. Phys.* **2008**, *128*, 44118.
(54) Comeau, D. C.; Bartlett, R. J. The Equation - of - Motion Coupled - Cluster method - applications to open-shell and closed-shell reference states. *Chem. Phys. Lett.* **1993**, *207*, 414−423.
(55) Stanton, J. F.; Bartlett, R. J. A Coupled-Cluster Based Effective Hamiltonian Method For Dynamic Electric Polarizabilities. *J. Chem. Phys.* **1993**, *99*, 5178−5183.
(56) Kasha, M. Characterization of electronic transitions in complex molecules. *Faraday Discuss.* **1950**, *9*, 14−19.
(57) Weigend, F.; Ahlrichs, R. Balanced basis sets of split valence, triple zeta valence and quadruple zeta valence quality for H to Rn: Design and assessment of accuracy. *Phys. Chem. Chem. Phys.* **2005**, *7*, 3297−3305.
(58) Ahlrichs, R.; Bar, M.; Haser, M.; Horn, H.; Kolmel, C. Electronic-structure calculations on workstation computers - the program system Turbomole. *Chem. Phys. Lett.* **1989**, *162*, 165−169.
(59) Furche, F.; Ahlrichs, R. Adiabatic time-dependent density functional methods for excited state properties. *J. Chem. Phys.* **2002**, *117*, 7433−7447.
(60) van Wuellen, C. Shared-Memory Parallelization of the TURBOMOLE Programs AOFORCE, ESCF, and EGRAD: How to Quickly Parallelize Legacy Code. *J. Comput. Chem.* **2011**, *32*, 1195−1201.
(61) Furche, F.; Ahlrichs, R.; Haettig, C.; Klopper, W.; Sierka, M.; Weigend, F. Turbomole. *WIREs Comput. Mol. Sci.* **2014**, *4*, 91−100.
(62) Schafer, A.; Horn, H.; Ahlrichs, R. Fully optimized contracted gaussian-basis sets for atoms Li to Kr. *J. Chem. Phys.* **1992**, *97*, 2571−2577.
(63) Valiev, M.; Bylaska, E. J.; Govind, N.; Kowalski, K.; Straatsma, T. P.; Van Dam, H. J. J.; Wang, D.; Nieplocha, J.; Apra, E.; Windus, T. L.; de Jong, W. A. NWChem: a comprehensive and scalable open-source solution for large scale molecular simulations. *Comput. Phys. Commun.* **2010**, *181*, 1477−1489.
(64) Humphrey, W.; Dalke, A.; Schulten, K. VMD: Visual Molecular Dynamics. *J. Mol. Graphics Modell.* **1996**, *14*, 33−38.
(65) Lin, C.-K.; Li, J.; Tu, Z.; Li, X.; Hayashi, M.; Lin, S. H. A theoretical search for stable bent and linear structures of low-lying electronic states of the titanium dioxide TiO_2 molecule. *RSC Adv.* **2011**, *1*, 1228−1236.
(66) Taylor, D. J.; Paterson, M. J. Vibronic coupling effects on the structure and spectroscopy of neutral and charged TiO_2 clusters. *Chem. Phys.* **2012**, *408*, 1−10.
(67) Wiggins, P.; Williams, J. A. G.; Tozer, D. J. Excited state surfaces in density functional theory: A new twist on an old problem. *J. Chem. Phys.* **2009**, *131*, 091101−091104.